JOURNAL OF THERMOPHYSICS AND HEAT TRANSFER
Vol. 15, No. 1, January–March 2001

Integral Calculations of Melt-Layer Heat Transfer in Aerodynamic Ablation

Chin-Yi Wei*
National Cheng-Kung University, Tainan 70101, Taiwan, Republic of China
and
Tse-Fou Zien†
Naval Surface Warfare Center, Dahlgren, Virginia 22448-5000

A theoretical analysis of a simple model for steady thermal ablation near the stagnation point of a blunt body in hypersonic flow is presented. The model consists of an inviscid flow downstream of the bow shock, a hot air boundary layer, a melt layer of the molten ablative, and the ablating solid. The different regions are properly coupled by the boundary conditions on the interfaces. The analysis is based on the similarity formulation of the governing equations of motion, and numerical solutions are obtained for the air boundary layer and the melt layer with relative ease. A procedure is presented for implementing the coupling of various regions, including the numerical solutions for the boundary layer and the melt layer. Typical results of the application of the procedure are presented to illustrate the solutions of the complete ablation problem based on the model; the solutions cover a wide range of the values of various ablation parameters. These solutions are compared with the Karman–Pohlhausen integral solutions presented earlier to assess the accuracy and the merits of the simpler integral method for such aerodynamic ablation problems. Some possible improvements on the integral method are suggested.

Nomenclature

A = dimensionless parameter; Eq. (33a)
A_{cp} = dimensionless parameter; Eq. (40a)
B = dimensionless parameter; Eq. (33b)
B^* = dimensionless parameter; Eq. (40b)
C = constant in the viscosity–temperature relation for air
C_p = specific heat at constant pressure
$\tilde{c}$ = constant defined in Eq. (17)
$E(1)$ = constant defined in Eq. (21b)
F_1 = x component of velocity in melt layer; Eq. (12)
F_2 = z component of velocity in melt layer; Eq. (10)
f_1 = similarity function in the air boundary layer; Eqs. (4) and (5)
f_2 = assumed solution in the melt layer; Eq. (41)
G_2 = dimensionless temperature in the melt layer; Eq. (18)
g_1 = dimensionless temperature in the air boundary layer, T/Te; Eqs. (4) and (5)
H_1 = total enthalpy of air in the freestream
$I(1)$ = constant defined in Eq. (21a)
K = effective Peclet number; Eq. (21c)
K_1 = constant parameter of melt layer; Eq. (14a)
K_2 = constant parameter of melt layer; Eq. (14b)
k = thermal conductivity
k_{2m} = thermal conductivity of melt layer on the ablation front
l = length scale for the air boundary layer; Eq. (26a)
M_∞ = freestream Mach number
m = dimensionless parameter; Eq. (34)
N = Newtonian flow parameter; Eq. (3)
N_m = dimensionless parameter for material properties in air and melt; Eq. (35)
Pr = Prandtl number
p = pressure
p_b = surface pressure near the stagnation point
Q_L = latent heat of solid per unit mass
$(\dot{q}_{12})_1$ = heat flux at air–melt interface (leaving air region)
$(\dot{q}_{12})_2$ = heat flux at air–melt interface (entering melt region)
$(\dot{q}_{23})_2$ = heat flux at melt–solid interface (leaving melt region)
R = radius of circular-nosed body
R^* = nondimensional temperature at air–melt interface, T^*/T_e
r = shielding factor; Eq. (22)
$\tilde{r}$ = modified shielding factor, $(k_2^*/k_{2m})r$
T = temperature
$(\boldsymbol{u}, \boldsymbol{w})$ = velocity vector
V = characteristic normal velocity in air boundary layer; Eq. (26b)
W_m = ablation speed
$\overline{W_m}$ = dimensionless ablation speed, W_m/V
(x, z) = Cartesian coordinate system fixed on ablation front
$\tilde{x}$ = x/z^*
z^* = melt-layer thickness
$\overline{z^*}$ = dimensionless melt-layer thickness, z^*/ℓ
α_1 = profile parameter of the air boundary layer
α_2 = profile parameter of the air boundary layer
α_3 = profile parameter of the melt layer
$\tilde{\alpha}$ = effective thermal diffusivity
β_1 = inviscid velocity gradient at the stagnation point
γ = specific heat ratio of the air
ε = (unknown) constant in the velocity at the air–melt interface
ε_A = (unknown) constant in the velocity at the air–melt interface; Eq. (39a)
ε_B = (unknown) constant in the velocity at the air–melt interface; Eq. (39b)
η_1 = modified similarity variable
η_2 = similarity variable in the melt layer, z/z^*
Θ = nondimensional temperature
μ = dynamic viscosity
ν = kinematic viscosity
$\overline{\nu_2}$ = average kinematic viscosity of the melt layer
ρ = density

Presented as Paper 2000-0205 at the 38th Aerospace Sciences Meeting, Reno, NV, 10–13 January 2000; received 15 February 2000; revision received 7 June 2000; accepted for publication 19 June 2000.

*Senior Research Staff, Institute of Aeronautics and Astronautics.
†Senior Research Scientist, System Research and Technology Department; also Visiting Professor, Institute of Aeronautics and Astronautics, National Cheng-Kung University, Tainan, Taiwan, Republic of China. Associate Fellow AIAA.

τ = shear stress
υ = ablation parameter, identical to $Q_L/c_3(T_m - T_i)$

Subscripts

e = conditions in the external inviscid flow
i = conditions of the solid far away from the ablating front
m = conditions on the ablation front
0 = conditions at the stagnation point for inviscid flow or at the ablation front, $z = 0$
1 = conditions in the air boundary layer
2 = conditions in the melt layer
3 = conditions in the ablating solid
∞ = conditions of freestream

Superscript

$*$ = conditions at the air–melt interface

I. Introduction

AERODYNAMIC ablation has long been recognized as one of the most challenging problems in aerodynamic heating. The nature of the physical phenomenon makes it necessary to couple the convection in the flowfield outside the ablating solid and the conduction, including phase changes, in the solid, in any meaningful theoretical analysis of the problem. In many important applications, there is also a melt layer formed by the molten ablative, for example, in the ablation of glassy materials as investigated by Hidalgo.[1] The interactions between the melt layer and the external airflow and the ablating solid play a significant role in the thermal protection of the solid structure and must be included in the analysis. Of course, there may be many other complex physical–chemical processes taking place in the ablating material, and their interactions with the flowfield make the problem even more difficult. Theoretical efforts aimed at providing a basic understanding of this extremely complex phenomenon and identifying important parameters of the problem for parametric studies often prove fruitful by developing relatively simple mathematical models to address the essential elements of the aerodynamic ablation phenomenon.

An effort in this direction was recently made by the present authors,[2] and some results were reported. In Ref. 2, a mathematical model is presented for simple aerodynamic ablation to study the basic elements of fluid dynamics and heat transfer associated with steady, thermal ablation in the neighborhood of the stagnation point of a two-dimensional body in hypersonic flight. A three-region structure is proposed (Fig. 1), including an indigenous melt layer of the molten ablative. The flowfield and heat transfer in the melt layer are carefully modeled and properly coupled to the air boundary layer and the ablating solid through boundary conditions on the interfaces. Parameters characterizing different regions of the model are identified. The mathematical problem admits a class of similarity solutions, and the theoretical analysis of the model can be carried out with relative ease. To facilitate the coupling of solutions of different regions to obtain the solutions of the whole ablation problem, analytical solutions for the boundary layer and the melt layer by the Karman–Pohlhausen (KP) type of integral method are also obtained. These analytical solutions exhibit an explicit dependence on the key parameters of the ablation model, and their use greatly reduces the computational efforts required to implement the coupling of the solutions for various regions. A procedure is then developed in Ref. 2 to carry out the coupling and to compute the approximate solutions of the whole ablation problem, and an example of the application of the procedure is presented to indicate the feasibility of obtaining such solutions. However, in the absence of the exact solutions of the model problem, it is difficult to assess the accuracy of the approximate solutions and to evaluate the validity of the KP method for such applications.

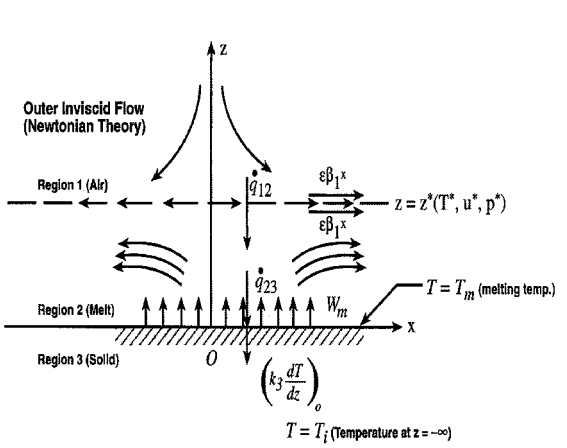

Fig. 1 Ablation model structure (coordinate system fixed on ablation front).

In the present paper, we will present a procedure for computing coupled solutions of the model problem, using the numerical solutions for the air boundary layer and the melt layer and the analytical solutions for the ablating solid. Extensive results of the application of the procedure will also be included. On the basis of these more exact calculations, the accuracy of the earlier approximate solutions will be assessed. Some preliminary results of the application of Zien's modified KP method (see, for example, Refs. 3 and 4) to the problem will also be presented and discussed. Finally, the merits and validity of integral methods, and the KP method in particular, for such aerodynamic ablation problems will be discussed.

II. Analysis

Results of Ref. 2 relevant to the present analysis will be briefly summarized for easy reference. Interested readers are referred to Ref. 2 for further details.

A. Inviscid Flow

The inviscid flow downstream of the bow shock is solved by using the well-known Newtonian theory for blunt bodies, and the surface pressure distribution near the stagnation point is given as follows[5,6]:

$$p_b(x) \cong p_{e0} - \rho_\infty u_\infty^2 x^2 \Big/ R^2 \tag{1}$$

where p_{e0} is the stagnation-point pressure in the Newtonian limit. We note that $\phi = x/R \to 0$, and also that $p_\infty \ll p_{e0}$ in this limit.

The inviscid pressure serves as the driving force for the entire flowfield of the ablation model, and it determines the inviscid velocity gradient at the stagnation point β_1, that is,

$$\beta_1 = \left(\frac{du_e}{dx}\right)_0 = \frac{u_\infty\sqrt{2(1+N)}}{RM_\infty} \tag{2}$$

In Eq. (2), N is the Newtonian flow parameter defined as

$$N = \frac{M_\infty^2(\gamma - 1)}{(\gamma + 1)} = \mathcal{O}(1) \tag{3}$$

B. Stagnation-Point Boundary Layer (Region 1)

In terms of the modified similarity variables ξ_1 and η_1, the momentum and energy equations pertaining to the self-similar hypersonic stagnation-point boundary layers are written in the following set of coupled ordinary differential equations for $f_1(\eta_1)$ and $g_1(\eta_1)$:

$$(Cf_1'')' + f_1 f_1'' + g_1 - (f_1')^2 = 0 \tag{4}$$

$$g_1'' + (Pr_1/C) f_1 g_1' = 0 \tag{5}$$

where $f_1(\eta_1)$ is related to the velocity $u(x, y)$ by

$$u = \beta_1 x f_1'(\eta_1) \tag{6}$$

and $g_1(\eta_1)$ is the nondimensional temperature, that is,

$$T/T_e = g_1(\eta_1) \tag{7}$$

where T_e is the temperature in the external inviscid flow. The appropriate boundary conditions for f_1 and g_1 are

$$f_1(0) = 0, \qquad f_1'(0) = \varepsilon, \qquad f_1'(\infty) = 1 \tag{8a}$$

$$g_1(0) = T^*/T_e \equiv R^*, \qquad g_1(\infty) = 1 \tag{8b}$$

where ε and R^* are unknown constants (see Ref. 2) to be determined by matching the solutions with the melt-layer solutions in region 2.

C. Melt Layer (Region 2)

The flow in this region is modeled as viscous and incompressible, and the conservation of mass and momentum can be expressed in terms of the following single nonlinear ordinary differential equation:

$$F_2'''' + K_2(F_2'F_2'' - F_2F_2''') = 0 \tag{9}$$

In the preceding equation, $F_2(\eta_2)$ is the dimensionless normal velocity defined by

$$w = W_m F_2(\eta_2) \tag{10}$$

where W_m is the constant (unknown) ablation velocity and η_2 is the similarity variable defined as

$$\eta_2 = z/z^* \tag{11}$$

with z^* denoting the (constant) unknown melt-layer thickness.

Note that, in deriving these results, we have assumed the x component of the velocity to be in the following form:

$$u = u^* F_1(\eta_2) \tag{12}$$

where $u^* = \varepsilon\beta_1 x$ is the air speed at the interface, $\eta_2 = 1$, and F_1 and F_2 are related by

$$F_2'(\eta_2) = -K_1 F_1(\eta_2) \tag{13}$$

so that the continuity equation can be satisfied. The constant parameters, K_1 and K_2, which characterize the melt-layer flow are defined, respectively, as follows:

$$K_1 = \varepsilon\beta_1 z^* \Big/ W_m \tag{14a}$$

$$K_2 \equiv W_m z^* \Big/ \overline{\nu_2} \tag{14b}$$

The boundary conditions for Eq. (9) are

$$F_2(0) = 1, \qquad F_2(1) = 0, \qquad F_2'(0) = 0, \qquad F_2'(1) = -K_1 \tag{15}$$

which satisfy the continuity of the velocity at the air–melt interface, $\eta_2 = 1$, and the no-slip condition at the ablation front, $\eta_2 = 0$.

Note that Eq. (9) can be integrated to give the following integral:

$$(F_2')^2 - F_2F_2'' + (1/K_2)F_2''' = \tilde{c} \tag{16}$$

where the constant $\tilde{c}$ can be determined by the boundary conditions, Eqs. (15), for example, at $\eta_2 = 1$. We obtain

$$\tilde{c} = K_1^2 + (1/K_2)F_2'''(1) \tag{17}$$

The constant $\tilde{c}$ appears in the melt-layer pressure field and is, therefore, an important parameter in coupling the melt-layer region and the air boundary layer. In this form, the x dependence of the melt flow is represented by u^* $(= \varepsilon\beta_1 x)$, as discussed in Ref. 2.

The energy equation can be solved analytically in terms of F_2, with the approximation that the dimensionless temperature Θ_2, defined as

$$\Theta_2(\eta_2) \equiv (T - T_m)\Big/\left(T^* - T_m\right) = G_2(\eta_2) \tag{18}$$

is only weakly dependent on x, that is, the thin melt-layer approximation. Thus, the equation for G_2 is given by

$$KF_2(\eta_2)\frac{\mathrm{d}G_2}{\mathrm{d}\eta_2} = \frac{\mathrm{d}^2G_2}{\mathrm{d}\eta_2^2} \tag{18a}$$

with $G_2(0) = 0$ and $G_2(1) = 1$. The solution is easily obtained as[2]

$$G_2(\eta_2) = I(\eta_2)/I(1) \tag{18b}$$

where

$$I(1) = \int_0^1 \exp\left(K\int_0^{\eta_2} F_2\,\mathrm{d}\eta_2\right)\mathrm{d}\eta_2 \tag{19a}$$

$$E(1) = \exp\left(K\int_0^1 F_2\,\mathrm{d}\eta_2\right) \tag{19b}$$

$$K \equiv \frac{W_m z^*}{\bar{\alpha}_2} \tag{19c}$$

K is the effective Peclet number of the melt layer.

The heat fluxes entering the melt layer, $(\dot{q}_{12})_2$, and leaving the melt-layer, $(\dot{q}_{23})_2$, are, respectively,

$$(\dot{q}_{12})_2 = \left[k_2^*\left(T^* - T_m\right)\Big/z^*\right][E(1)/I(1)] \tag{20}$$

$$(\dot{q}_{23})_2 = \left[k_{2m}\left(T^* - T_m\right)\Big/z^*\right][1/I(1)] \tag{21}$$

The shielding factor r, defined as

$$r = \frac{(\dot{q}_{23})_2}{(\dot{q}_{12})_2} \tag{22}$$

is given by

$$r = \left(k_{2m}\Big/k_2^*\right)[1/E(1)] \tag{23a}$$

and the modified shielding factor, $\tilde{r} = r(k_2^*/k_{2m})$, is given by

$$\tilde{r} = 1/E(1) = \tilde{r}(K, K_1, K_2) \tag{23b}$$

Note that the shielding factor measures the effectiveness of the melt layer in reducing the thermal load on the solid structure, and it, of course, depends on the fluid dynamic and heat transfer properties of the layer as characterized by the parameters K, K_1, and K_2.

D. Ablating Solid (Region 3)

Assuming a one-dimensional heat conduction model for the ablating solid, we can obtain the temperature distribution in a simple closed form.[2] The result is

$$\Theta_3 = (T - T_i)/(T_m - T_i) = \exp(W_m z/\bar{\alpha}_3) \tag{24}$$

where T_i is the temperature of the solid far away from the ablating front, $z = 0$. The energy balance on the ablation surface provides the coupling between the melt layer and the ablating solid, that is,

$$(\dot{q}_{23})_2 = c_3\rho_3 W_m(T_m - T_i)(1 + \upsilon) \tag{25}$$

where $\upsilon \equiv Q_L/c_3(T_m - T_i)$ is an ablation parameter.

Note that the heat conduction in the solid is modeled as one dimensional, for simplicity. This simplifying assumption is consistent with the approximation that the temperature field in the external melt layer is only weakly dependent on x, as discussed earlier.

E. Length and Velocity Scales

For computational convenience, dimensionless quantities will be used. Thus, we introduce the reference length l and reference velocity V as

$$\ell = \left(\nu_1^*\Big/\beta_1\right)^{\frac{1}{2}} \tag{26a}$$

$$V = \left(\beta_1\nu_1^*\right)^{\frac{1}{2}} \tag{26b}$$

Using l and V, we define dimensionless melt-layer thickness $\overline{z^*}$ and dimensionless ablation speed $\overline{W_m}$ as follows:

$$\overline{z^*} = z^*/\ell \tag{27a}$$

$$\overline{W_m} = W_m/V \tag{27b}$$

F. Coupling

The interface boundary conditions at the air–melt interface, $z = z^*$, are continuity of velocity and temperature, which have already been incorporated into the formulation of the problem. Additional matching conditions are $(\dot{q}_{12})_1 = (\dot{q}_{12})_2$, $p_b(x) = p_2^*(x)$, and $\tau_1^* = \tau_2^*$, in parentheses, that is (shear-stress continuity). These conditions lead to the following equations:

$$\frac{C_{p2}}{C_{p1}} A = \frac{Pr_2}{Pr_1}\frac{\mu_1^*}{\mu_2^*}\frac{I(1)}{E(1)}\overline{z^*} g_1'(0) \tag{28}$$

$$\varepsilon = M_\infty \left(\frac{\rho_\infty}{\rho_2}\frac{K_1^2}{\tilde{c}}\frac{1}{1+N}\right)^{\frac{1}{2}} \tag{29}$$

$$\overline{z^*} = -\varepsilon \frac{\mu_2^*}{\mu_1^*}\frac{1}{K_1}\frac{F_2''(1)}{f_1'(0)} \tag{30}$$

The energy balance on the melt–solid interface, Eq. (25), can be written in terms of the dimensionless quantities as follows:

$$B\frac{\nu_1^* k_{2m}}{c_3 \rho_3} = \overline{W_m}\,\overline{z^*} I(1) \tag{31}$$

Also, Eqs. (14a) and (14b) can be rewritten in terms of $\overline{z^*}$ and $\overline{W_m}$ as

$$K_1 = \varepsilon\left(\overline{z^*}\Big/\overline{W_m}\right) \tag{32a}$$

$$K_2 = \overline{W_m}\,\overline{z^*}\left(\nu_1^*\Big/\overline{\nu_2}\right) \tag{32b}$$

Equations (17) and (28–32b) form a system of seven equations for the seven unknowns, that is, ε, R^*, K_1, K_2, $\tilde{c}$, $\overline{z^*}$, and $\overline{W_m}$, given the freestream conditions and the properties of the materials involved.

In the preceding system of equations, we have introduced two additional dimensionless parameters, A and B, that relate, respectively, to the freestream energy level T_{eo} and the thermal potential of the original ablative $(T_m - T_i)$. They are defined by

$$A \equiv \left(T^* - T_m\right)\Big/T_{eo} \tag{33a}$$

$$B \equiv \left[\left(T^* - T_m\right)\Big/(T_m - T_i)\right][1/(1+\upsilon)] \tag{33b}$$

Note that in deriving Eq. (28) we have used $H_1 = C_{p1} T_{eo}$, where H_1 is the total energy of the freestream.

III. Coupling Procedure

The system of Eqs. (17) and (28–32b) includes quantities $f_1''(0)$, $g_1'(0)$, $F_2(\eta_2)$, $F_2''(1)$, and $F_2'''(1)$ that are part of the solutions of the differential equations (4), (5), and (9). Numerical solutions of these were obtained in Ref. 2, but the coupling was accomplished using the KP integral solutions for regions 1 and 2. The required computation of the approximate solutions was relatively easy, owing to the explicit dependence of the approximate solutions on various parameters.

In this paper, we will present a procedure for the coupling based on the numerical solutions for the air boundary layer and the melt layer. The complete solutions are, therefore, more accurate than those presented in Ref. 2, and they can be used to determine the accuracy of the previous solutions. On the basis of the comparison, the relative merits of the KP method for the aerodynamic ablation problems can be reasonably assessed.

To proceed, we will follow the inverse approach, which was conveniently used in Ref. 2 by specifying a set of values for ε and R^* and obtaining the solutions for the parameters A and B. Unlike the procedure of Ref. 2, the present procedure necessarily involves the solutions of the differential equations and their boundary conditions, Eqs. (4), (5), (8), (9), and (15), in its iteration process, and the computational labor is obviously greater. However, the procedure can be made more efficient if use is made of the KP solution as the initial guess.

To be consistent with the notations used in Ref. 2, we introduce the following parameters in the computation:

$$m = M_\infty^2(\rho_\infty/\rho_2)[1/(1+N)] \tag{34}$$

$$N_m = \left(\bar{\nu}_2\Big/\nu_1^*\right)\left(\mu_1^*\Big/\mu_2^*\right)^2 \tag{35}$$

Equation (29) can be rewritten as

$$\varepsilon^2 = m\left\{K_1^2\Big/\left[K_1^2 + F_2'''(1)/K_2\right]\right\} \tag{36}$$

where Eq. (17) was used.

Equations (32a) and (32b) and Eq. (30) can be combined to give the following equation:

$$\varepsilon^2 = \left\{N_m K_1^3 K_2\left[\frac{f_1''(0)}{F_2''(1)}\right]^2\right\}^{\frac{2}{3}} \tag{37}$$

Equations (36) and (37) form the basis of the iteration in the present procedure. The computational procedure is outlined as follows:

1) Assign a set of values to ε and R^*, and solve Eqs. (4), (5), and (8) for $f_1(\eta_1;\, \varepsilon,\, R^*)$ and $g_1(\eta_1;\, \varepsilon,\, R^*)$, numerically, by the well-known fourth Runge–Kutta shooting method, as in Ref. 2.

2) Also, for the values of ε and R^* chosen in step 1 and the prescribed values of m and N_m, obtain the KP solution of the coupled ablation problem by the procedure of Ref. 2. Specifically, for given values of ε, R^*, and m, the previous KP procedure gives solutions of K_1 and K_2 as functions of N_m (see, for example, Fig. 8 of Ref. 2). Therefore, we have the following results from the KP coupling procedure used in Ref. 2:

$$K_1 = K_1\left(N_m;\, \varepsilon,\, R^*,\, m\right) \tag{38a}$$

$$K_2 = K_2\left(N_m;\, \varepsilon,\, R^*,\, m\right) \tag{38b}$$

The values of K_1 and K_2 will be used as the initial guesses for the present iteration procedure.

3) Use the values of K_1 and K_2 obtained in step 2 in the numerical solution of Eqs. (9) and (15) for $F_2(\eta_2;\, K_1,\, K_2)$. Again, the fourth-order Runge–Kutta shooting method is used. Calculate the corresponding ε by Eqs. (36) and (37), respectively, to give

$$\varepsilon_A^2 = m\left\{K_1^2\Big/\left[K_1^2 + F_2'''(1)/K_2\right]\right\} \tag{39a}$$

$$\varepsilon_B^2 = \left\{N_m K_1^3 K_2\left[\frac{f_1''(0)}{F_2''(1)}\right]^2\right\}^{\frac{2}{3}} \tag{39b}$$

based on the values of $f_1''(0)$ obtained in step 1 and $F_2''(1)$ and $F_2'''(1)$ obtained in step 3.

4) Using the differences in ε, $\Delta\varepsilon_A = |\varepsilon - \varepsilon_A|$ and $\Delta\varepsilon_B = |\varepsilon - \varepsilon_B|$, as a measure of convergence, repeat step 3 by choosing new values of K_1 and K_2 as $(K_{1i},\, K_{2j}) = (K_1 + i\Delta K_1,\, K_2 + j\Delta K_2)$ where i and j are integers increasing from 1 to 10 and ΔK_1 and ΔK_2 are some appropriate increments of K_1 and K_2 in the iteration. The criteria used for convergence in the present computations are arbitrarily set at $\Delta\varepsilon_A$ and $\Delta\varepsilon_B < 10^{-6}$.

5) When the convergence criteria are met, the corresponding values of K_1 and K_2 are accepted as the coupled solutions from which $F_2(\eta_2;\, K_1,\, K_2)$, $I(1)$, and $E(1)$ are calculated. The melt-layer flow is, thus, determined for a set of given values of the parameters ε, R^*, m, and N_m.

6) Equations (32a) and (32b) are used to give the solutions of $\overline{z^*}$ and $\overline{W_m}$, and finally Eqs. (28) and (31) are used to give solutions for A and B as

$$A_{\text{cp}} \equiv \frac{C_{p2}}{C_{p1}} A \tag{40a}$$

$$B^* \equiv B\left(\frac{\nu_1^* k_{2m}}{c_3 \rho_3}\right) \tag{40b}$$

7) To fix the idea, all of the calculations in the present paper are based on Pr_1, Pr_2, c, and $\overline{\nu_2^*/\nu_1^*} = 0.7$, 0.5, 1.0, and 2.5×10^{-4}, respectively.

IV. Results and Discussion

The coupling procedure was carried out successfully in the present investigation, and converged solutions were obtained over a wide range of the parameters, ε, R^*, m, and N_m. The ranges of the parameters covered are $0.06 \le R^* \le 1.0$, $0.05 \le \varepsilon \le 0.28$, $0.05 \le m \le 1.0$, and $0.05 \times 10^{-6} \le N_m \le 0.05$. Selected results are presented in this paper, along with the corresponding results obtained using the previous KP coupling procedure of Ref. 2. The accuracy of the KP coupling results can, thus, be discussed on the basis of the comparison. Following the presentation used in Ref. 2, we will use N_m as the independent parameter in presenting the present results, with ε and $R^* = 0.2$ and 0.4 and $m = 0.1$ and 0.2.

A. Melt-Layer Profiles

We solved Eqs. (9) and (15) numerically to obtain the melt-layer profiles $F_2(\eta_2)$, $F_1(\eta_2)$, and $G_2(\eta_2)$ for some given values of K_1 and K_2. The purpose is to determine the sensitivity of the profiles to the parameters K_1 and K_2, which are the basic quantities obtained in the coupling scheme. Typical results are presented in Figs. 2a and 2b. Figure 2a shows the dependence of the profiles on K_2 for a fixed value of $K_1 = 1.52$, and Fig. 2b shows the profile dependence on K_1 for a fixed values of $K_2 = 0.65$. The results indicate that the effect of

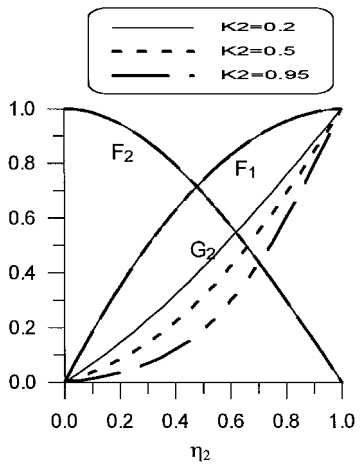

a) $K_1 = 1.52$

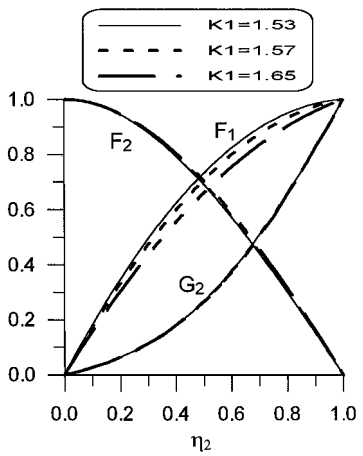

b) $K_2 = 0.65$

Fig. 2 Numerical solutions for melt-layer profiles dependence on K_1 and K_2.

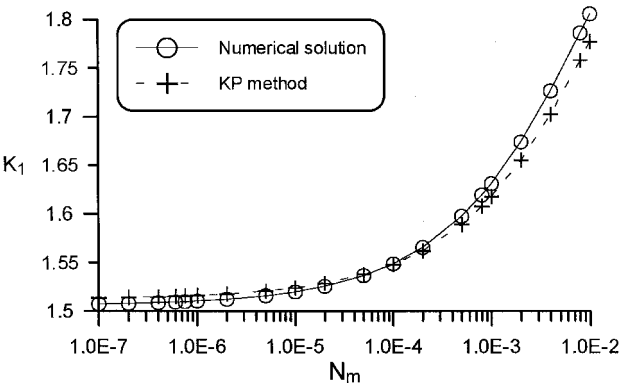

a) $K_1(N_m)$

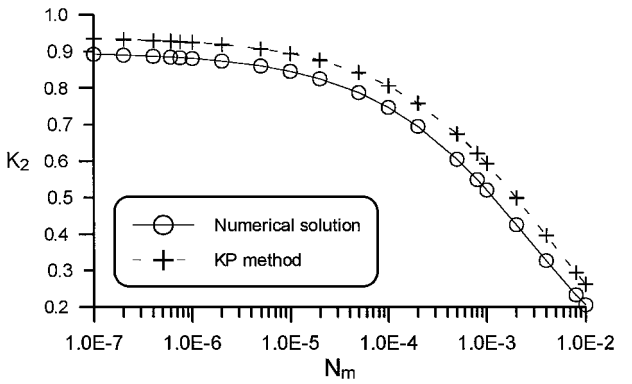

b) $K_2(N_m)$

Fig. 3 Coupled solutions of model ablation problem, ε, R^*, and m = 0.2, 0.4, and 0.1.

K_2 on G_2 is much more pronounced than on F_1 and F_2 (Fig. 2a) and that the dependence of F_1 on K_1 is much stronger than that of F_2 and G_2 (Fig. 2b). The result is to be expected in view of the explicit dependence of F_1 and K_1 as shown in Eq. (13) and the explicit dependence of G_2 and K_2 in the analytical solution of G_2 (see Ref. 2, note that $K = Pr_2 K_2$). However, note that in either case, the profile dependence on the parameters K_1 and K_2 is only moderate.

B. Coupling Parameters K_1 and K_2

Figures 3a, 3b, 4a, and 4b show the basic results of the coupling given in terms of the melt-layer parameters K_1 and K_2 as functions of N_m for given values of the parameters ε, R^*, and m that characterize the air boundary layer. Figure 3a shows the results of K_1, and Fig. 3b shows the results of K_2 for ε, R^*, and $m = 0.2$, 0.4, 0.1. Both the present solutions and the previous KP solutions are included. Figures 4a and 4b show similar results, but for $m = 0.2$. It appears from these results that the KP solutions are reasonably accurate for a wide range of N_m, at least for the values of ε, R^*, and m used in the computation.

C. Melt-Layer Profiles

The melt-layer profiles, F_1 , F_2, and G_2 , of the coupled solutions are shown in Figs. 5 and 6 corresponding, respectively, to ε, R^*, m, and $N_m = 0.2$, 0.4, 0.1, and 0.75×10^{-6} and 0.2, 0.4, 0.2, and 0.75×10^{-6}. It is clear that the KP solutions agree exceedingly well with the numerical solutions in both cases. This can be explained by the weak dependence of the profiles on K_1 and K_2 as discussed in Sec. IV.A, noting that the coupled KP solutions of K_1 and K_2 are in good agreement with those of the coupled numerical solutions (Figs. 3 and 4).

D. Solutions of the Selected Examples

The rest of the solutions of the inverse problem, A_{cp}, B^*, $\tilde{r}$, $\overline{z^*}$, and $\overline{W_m}$, are shown in Figs. 7–10. Again, the corresponding solutions

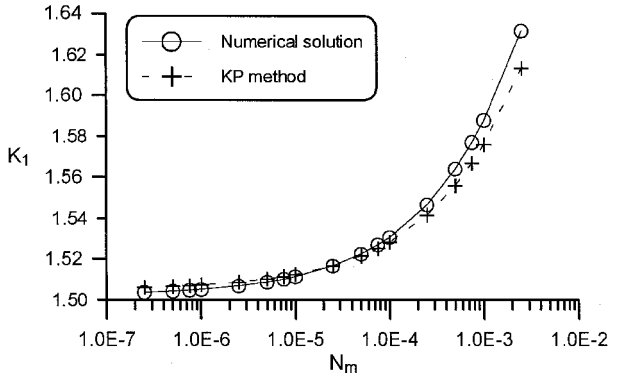

a) $K_1(N_m)$

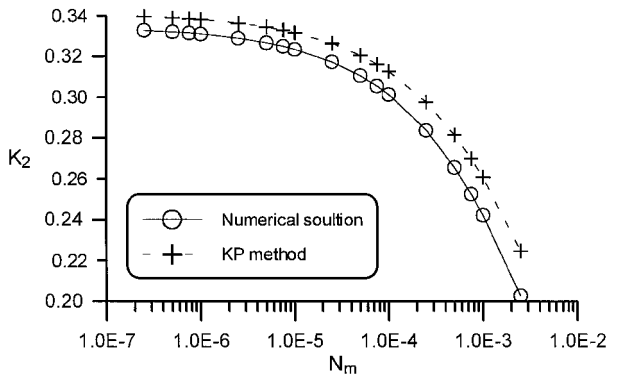

b) $K_2(N_m)$

Fig. 4 Coupled solutions of model ablation problem, ε, R^*, and m = 0.2, 0.4, and 0.2.

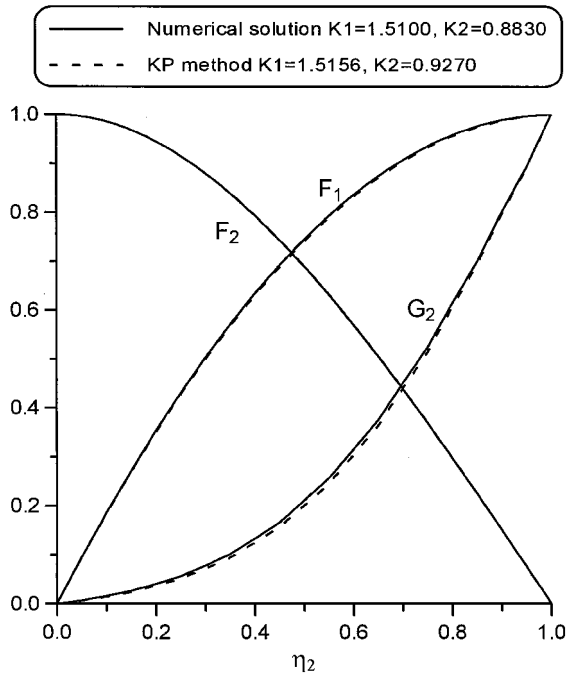

Fig. 5 Melt-layer profiles, coupled solutions, ε, R^*, m, and N_m = 0.2, 0.4, 0.1, and 0.75 × 10^{-6}.

by the previous KP coupling procedure are also included for comparison, and results are presented for ε, R^*, and $m = 0.2$, 0.4, and 0.1 in Figs. 7a and 7b and 8a–8c and for ε, R^*, and $m = 0.2$, 0.4, and 0.2 in Figs. 9a and 9b and 10a–10c. The approximate KP solutions of $\overline{z^*}$ and $\overline{W_m}$ are seen to compare favorably with those of the numerical solutions in the range of parameters covered in the study. However, the accuracy of the KP solutions for A_{cp} is found to be not as good, especially for larger values of N_m. This is because the

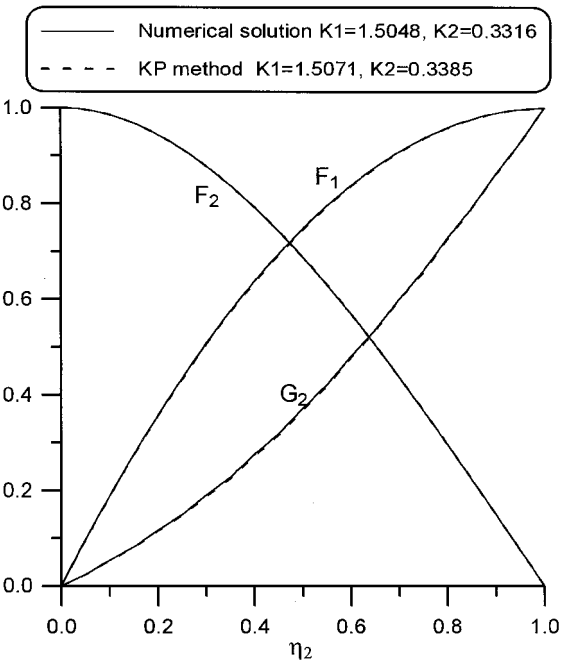

Fig. 6 Melt-layer profiles, coupled solutions, ε, R^*, m, and N_m = 0.2, 0.4, 0.2, and 0.75 × 10^{-6}.

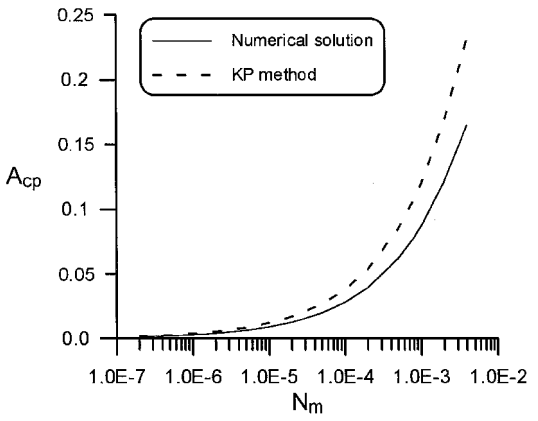

a) A_{cp} (N_m)

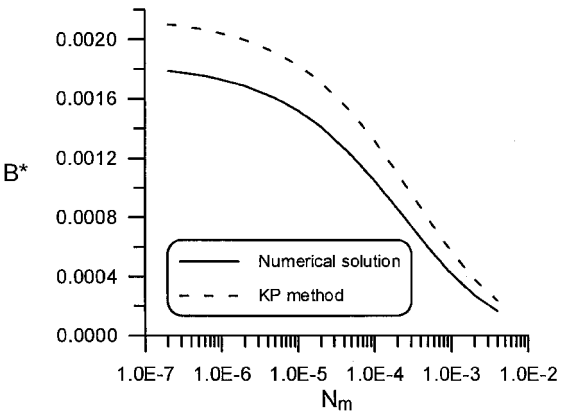

b) B^* (N_m)

Fig. 7 Solutions of A_{cp} and B^* as functions of N_m; ε, R^*, and m = 0.2, 0.4, and 0.1.

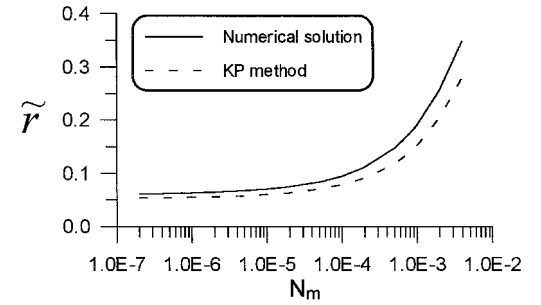

a) $\tilde{r}$ (N_m)

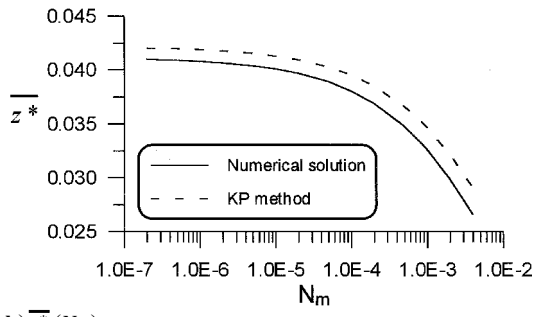

b) $\overline{z^*}$ (N_m)

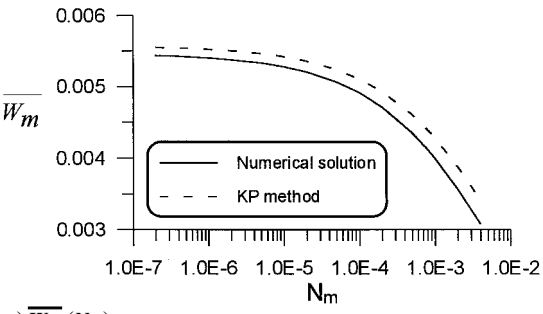

c) $\overline{W_m}$ (N_m)

Fig. 8 Solutions of $\tilde{r}$, $\overline{z^*}$, and $\overline{W_m}$ as functions of N_m; ε, R^*, and m = 0.2, 0.4, and 0.1.

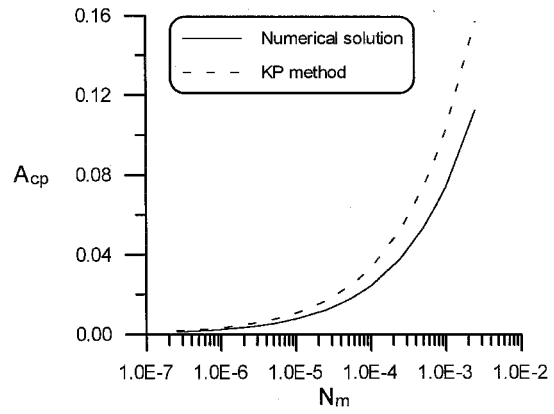

a) $A_{cp}(N_m)$

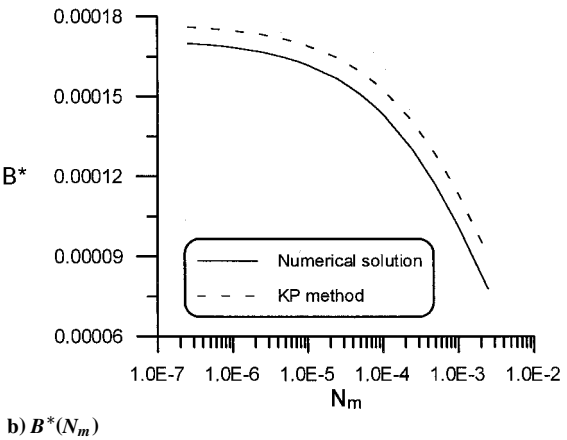

b) $B^*(N_m)$

Fig. 9 Solutions of A_{cp} and B^* as functions of N_m; ε, R^*, and m = 0.2, 0.4, and 0.2.

quantity A_{cp} depends directly on $g'(0)$ [Eq. (28)], which was not predicted accurately by the KP method (see Ref. 2). The need for an improved KP method for the approximate solution of the problem is, thus, suggested.

V. Refined KP Method

As was demonstrated in Ref. 2, the implementation of the coupling procedure for the three main regions of the present ablation model can be made much easier by using the analytical solutions of the KP integral method for the air boundary layer and the melt layer. The results presented in this paper provide additional evidence of the merits of the integral method. However, as was discussed in Sec. IV, in the calculation of certain quantities of the model, an improvement in the accuracy of the KP method still appears desirable. In the present study, an effort in this direction is also made by applying the refined KP method developed by Zien (see, for example, Refs. 3 and 4) to the solutions of the melt-layer flow and heat transfer, and some preliminary results will be discussed here. We note that some integral solutions of the air boundary layer (region 1) by Zien's method have already been presented and discussed in Ref. 2.

Briefly, the refined KP method attempts to improve the accuracy of the boundary derivative of the solution of a given differential equation. It makes a combined use of the integral of the original differential equation and the integral of a moment of the original equation.[3,4] By doing so, the boundary derivative of the solution can be calculated on the basis of some integrals involving the approximate solution assumed in the method, instead of directly taking the derivative of the approximate solution itself. Physically, the idea is to base the evaluation of the boundary derivative, which usually represents some kind of flux (moment or energy) at the boundary, on the appropriate conservation law for the given domain under consideration. Better accuracy is, thus, expected as a result.

In the present ablation model, coupling between the melt layer and the air boundary layer involves boundary derivatives $F_2'''(1)$ and $F_2''(1)$ [Eqs. (17) and (30)], and their accuracy will obviously affect the accuracy of the complete coupled solution of the ablation problem. In the following, we will use the refined KP method to calculated the boundary derivative $F_2'''(1)$ of the differential equation, Eq. (9), and its boundary conditions, Eq. (15). Other boundary derivatives appear in the solution process. For this reason, we refer to the results obtained as preliminary. Further improvements are possible and should be carried out to exploit the full potential of the ideas underlying the refined KP method.

To proceed, we first assume an approximate solution of the following polynomial form:

$$f_2(\eta_2) = 1 + (-3 + K_1 + \alpha_3)\eta_2^2 + (2 - K_1 - 2\alpha_3)\eta_2^3 + \alpha_3\eta_2^4 \quad (41)$$

The assumed solution [Eq. (41)] satisfies the boundary conditions [Eq. (15)].

Integration of Eq. (9) gives

$$F_2'''(1) = F_2'''(0) - K_2 \int_0^1 (F_2' F_2'' - F_2 F_2''')\, \mathrm{d}\eta_2 \quad (42)$$

After integration by parts and making use of the boundary conditions [Eq. (15)], we have

$$F_2'''(1) = F_2'''(0) - K_2 K_1^2 - K_2 F_2''(0) \quad (43)$$

In the classical KP method, Eq. (43) alone determines the solution parameter α_3, after substituting f_2 for F_2. The boundary derivatives

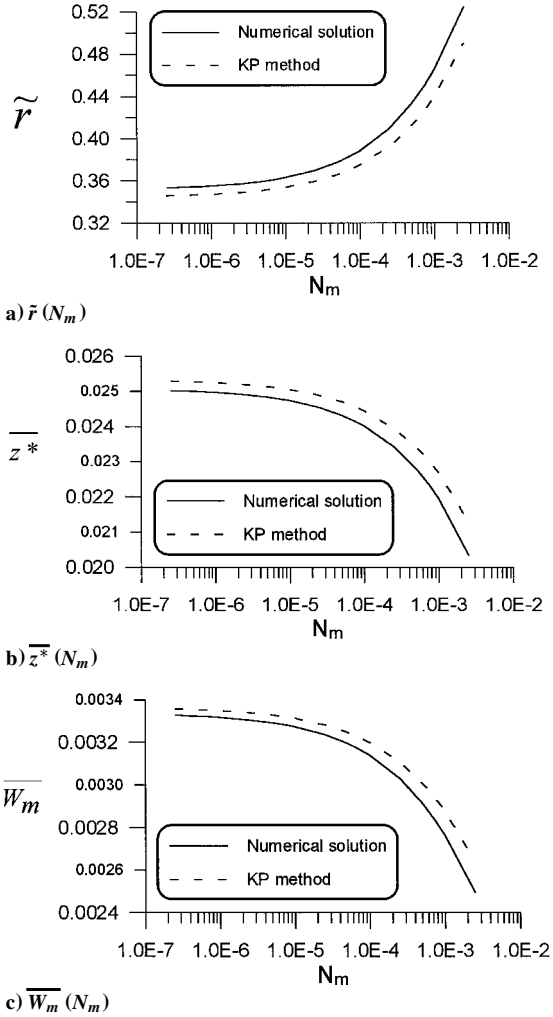

Fig. 10 Solutions of $\tilde{r}$, $\overline{z^*}$, and $\overline{W_m}$ as functions of N_m; ε, R^*, and $m = 0.2$, 0.4, and 0.2.

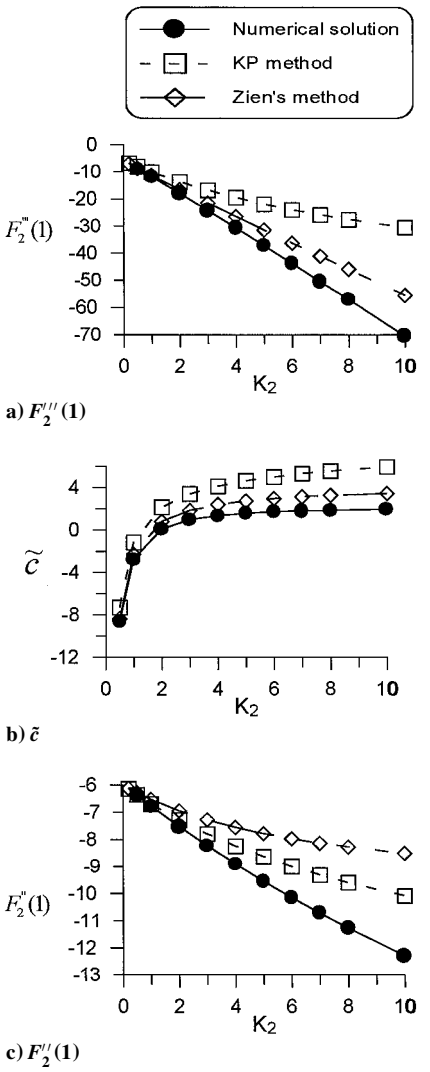

Fig. 11 Boundary derivatives of melt-layer velocity, $K_1 = 3$.

are obtained directly by taking derivatives of the approximate solution f_2. Specifically,

$$F_2'''(1) = f_2'''(1) = 6(2 - K_1 + 2\alpha_3) \tag{44}$$

In the present refined KP method, Eq. (43) is used only as an expression for the boundary derivative $F_2'''(1)$, and a second equation is generated by integrating the η_2 moment of Eq. (9), that is,

$$F_2'''(1) - F_2''(1) + F_2''(0) + K_2K_1^2 - 2K_2\int_0^1 (F_2')^2\,\mathrm{d}\eta_2 \tag{45}$$

We use Eqs. (43) and (45) to determine the solution parameter α_3 and the boundary derivative $F_2''(1)$ with the substitution $F_2 = f_2$ for all other terms in these two equations. Note that the other boundary derivatives including $F_2''(1)$ are still calculated by directly taking the derivative of the approximation solution f_2, for example,

$$F_2''(1) = f_2''(1), \qquad \text{etc.} \tag{46}$$

after α_3 is determined.

To improve the accuracy of the boundary derivatives further, we can generate more moment-like equations so that taking derivatives of the approximate solution can be avoided to the extent desired. This may be a worthwhile study to pursue in the future.

For the present application of the refined KP method, we have the following equations derived from Eq. (43) and Eq. (46), respectively,

$$F_2'''(1) = 12 - 6(K_1 - K_2) - K_1K_2(2 + K_1) - 2(6 + K_2)\alpha_3 \tag{47}$$

$$\tfrac{1}{7}K_2\alpha_3^2 - \left(45 + \tfrac{15}{2}K_2 - \tfrac{1}{2}K_1K_2\right)\alpha_3 + K_2\left(\tfrac{27}{2} - 6K_1 - K_1^2\right) = 0 \tag{48}$$

For a given set of values for K_1 and K_2, Eqs. (47) and (48) determine the solution parameter α_3 and the boundary derivative $F_2'''(1)$.

Figures 11 and 12 give some preliminary results of the application of the refined KP method (Zien's[3,4] method) to the calculation of boundary derivatives of the melt-layer flow equation, Eqs. (9) and (15). Numerical solutions and the classical KP solutions are also included for comparison. Results of $F_2'''(1)$, $F_2''(1)$, and $\tilde{c}$ are presented as functions of K_2 for the fixed values of $K_1 = 3$ (Fig. 11) and $K_1 = 2$ (Fig. 12). Note that the results of $F_2''(1)$, though denoted as Zien's solutions in Figs. 11c and 12c, are actually obtained by taking direct derivative of the approximate solution f_2 [see Eq. (46)].

Figures 11a, 11b, 12a, and 12b show clearly that the results of $F_2'''(1)$ and $\tilde{c}$ calculated by the refined KP method are superior to those calculated by the classical KP method, as expected. However the corresponding results of $F_2''(1)$ presented in Figs. 11c and 12c are less satisfactory. The difficulty can be attributed to the way $F_2''(1)$ is calculated, as was noted. This finding points to the need for additional moment equations for use in the refined KP method to avoid taking the direct derivative of the approximate solution in calculating any boundary derivatives. The implementation of the coupling procedure using the Zien's solutions[3,4] for the air boundary layer and the melt layer will not be pursued until an appropriate improvement in $F_2''(1)$ calculations is achieved.

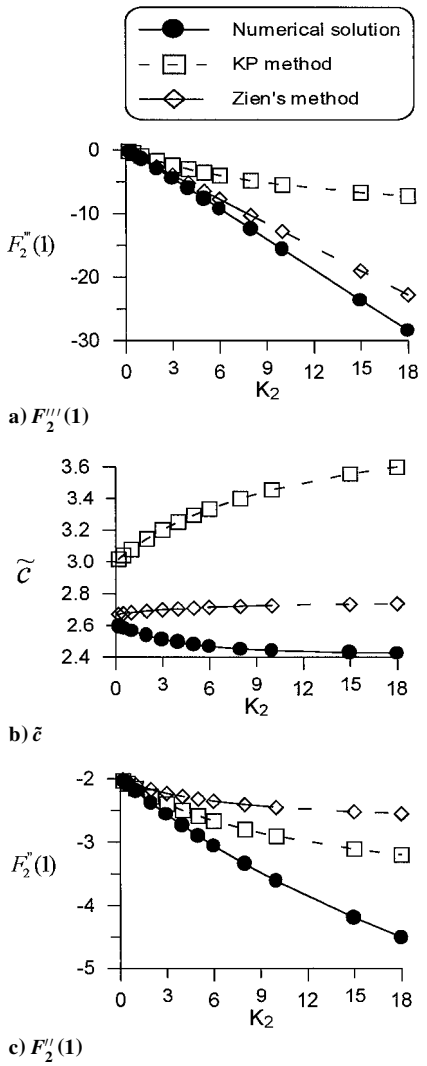

Fig. 12 Boundary derivatives of melt-layer velocity, $K_1 = 2$.

VI. Application

It is believed that the relatively simple solution of the ablation flowfield presented here and in Ref. 2 can perhaps be used as a starting point in the study of the effects of particles/droplets in the gas stream, for example, aluminum oxide particles in the solid rocket exhaust in the operation of vertical missile launchers. Here one can consider the case of a small particle volumetric fraction so that the particle effects can be treated as a small perturbation to the basic ablation flowfield. The dynamic and thermal behavior of the particles can then be studied as they travel through a given flow and thermal field, and a simplified form of the mechanical erosion/ablation problem (see, for example, Cheung et al.[7]) can be conveniently studied.

VII. Concluding Remarks

On the basis of the comparison of the present results and the KP results reported in Ref. 2 for the coupled ablation problem, the accuracy of the approximate KP solutions has been reasonably assessed. The simplicity of the KP method makes it a valuable tool for engineering estimates of various ablation parameters for preliminary design studies, and the KP solutions also prove to be useful as initial guesses in the iteration process of the present procedure of coupling the numerical solutions for different regions. In this regard, note that the converged solution obtained in the present studies of coupling numerical solutions corresponds only to the initial guess provided by the approximate KP solution. The question of uniqueness of the present solution is difficult to address. With the solution procedure being an inverse approach in nature, the errors in the approximate integral solution are given in terms of the freestream and initial conditions A and B, and it is not obvious how to infer the corresponding errors in the solutions of the direct problem ε, R^*, z^*, etc., from the errors in the present inverse solution. Also, it would be interesting and useful to apply the present nondimensional results to a practical case of melting ablation and present the corresponding results in dimensional form. This task, while straightforward, will require the data of transport/thermodynamic properties of the materials pertinent to the model, and it will be carried out in a future study.

An effort to improve the accuracy of the KP solution is made by applying Zien's[3,4] refined KP method, but some preliminary results indicate that additional moment equations are perhaps needed in the application of the method to accomplish the objective. This means that the possible improvement will be at the expense of the simplicity of the original integral method.

Acknowledgments

The research of T. F. Zien was supported by the Naval Surface Warfare Center, Dahlgren Division's In-House Laboratory Independent Research Program, and we would like to thank T. K. Chu, Program Manager, for his support.

References

[1]Hidalgo, H., "Ablation of Glassy Material Around Blunt Bodies of Revolution," *ARS Journal*, Vol. 30, Sept. 1960, pp. 806–814.

[2]Zien, T. F., and Wei, C. Y., "Heat Transfer in the Melt Layer of a Simple Ablation Model," *Journal of Thermophysics and Heat Transfer*, Vol. 13, No. 4, 1999, pp. 450–459.

[3]Zien, T. F., "Approximate Analysis of Heat Transfer in Transpired Boundary Layers with Effects of Prandtl Number," *International Journal of Heat and Mass Transfer*, Vol. 19, No. 5, 1976, pp. 513–521.

[4]Zien, T. F., "Integral Solutions of Ablation Problems with Time-Dependent Heat Flux," *AIAA Journal*, Vol. 16, No. 12, 1978, pp. 1287–1295.

[5]Anderson, J. D., *Hypersonic and High-Temperature Gas Dynamics*, McGraw–Hill, New York, 1989, Chaps. 3 and 9.

[6]Rasmussen, M., *Hypersonic Flow*, Wiley, New York, 1994, Chap. 9.

[7]Cheung, F. B., Yang, B. C., Burch, R. L., and Koo, J. H., "Effect of Melt-Layer Formation on Thermo-Mechanical Erosion of High-Temperature Ablative Materials," *Proceedings of 1st Pacific International Conference on Aerospace Science and Technology*, National Cheng-Kung University, Tainan, Taiwan, ROC, 1993, pp. 302–309.